NeuroImage **17,** 1117–1130 (2002)
doi:10.1006/nimg.2002.1282

# Linking Physics with Physiology in TMS: A Sphere Field Model to Determine the Cortical Stimulation Site in TMS

Axel Thielscher*[,1] and Thomas Kammer†

**Department of Psychiatry III, University of Ulm, Ulm, Germany and †Department of Neurobiology, Max-Planck-Institute for Biological Cybernetics, Tübingen, Germany*

Received April 10, 2002

**A fundamental problem of transcranial magnetic stimulation (TMS) is determining the site and size of the stimulated cortical area. In the motor system, the most common procedure for this is motor mapping. The obtained two-dimensional distribution of coil positions with associated muscle responses is used to calculate a center of gravity on the skull. However, even in motor mapping the exact stimulation site on the cortex is not known and only rough estimates of its size are possible. We report a new method which combines physiological measurements with a physical model used to predict the electric field induced by the TMS coil. In four subjects motor responses in a small hand muscle were mapped with 9–13 stimulation sites at the head perpendicular to the central sulcus in order to keep the induced current direction constant in a given cortical region of interest. Input–output functions from these head locations were used to determine stimulator intensities that elicit half-maximal muscle responses. Based on these stimulator intensities the field distribution on the individual cortical surface was calculated as rendered from anatomical MR data. The region on the cortical surface in which the different stimulation sites produced the same electric field strength (minimal variance, 4.2 ± 0.8%.) was determined as the most likely stimulation site on the cortex. In all subjects, it was located at the lateral part of the hand knob in the motor cortex. Comparisons of model calculations with the solutions obtained in this manner reveal that the stimulated cortex area innervating the target muscle is substantially smaller than the size of the electric field induced by the coil. Our results help to resolve fundamental questions raised by motor mapping studies as well as motor threshold measurements.** 

[1] To whom correspondence and reprint requests should be addressed at Abteilung Psychiatrie III, Universität Ulm, Leimgrubenweg 12-14, D- 89075 Ulm, Germany. Fax: +49 731 50026751. E-mail: axel.thielscher@medizin.uni-ulm.de.

***Key Words:*** **electromagnetic fields; motor cortex; motor mapping; sphere model; transcranial magnetic stimulation.**

## INTRODUCTION

Transcranial magnetic stimulation (TMS) is a widely used research tool in the neurosciences (Hallett, 2000; Walsh and Cowey, 2000). In conjunction with stereotactic coil positioning devices, it allows us to stimulate cortical sites on an individual anatomical basis (Krings *et al.*, 1997; Herwig *et al.*, 2001; Kammer *et al.*, 2001). However, the exact size and site of the stimulated neural tissue is not known, even in stereotactically navigated TMS. A common procedure for determining a stimulation site is systematic mapping of muscle responses as a function of the coil position over the primary motor cortex (motor mapping) (Wassermann *et al.*, 1992; Wilson *et al.*, 1993). The two-dimensional map showing the strength of the muscle responses at each coil position is used to calculate a center of gravity (COG) on the skull. That site on the cortex that is closest to the COG on the skull is commonly referred to as the probable cortical representation of the target muscle. However, the extension of the cortical representation cannot be assessed by motor mapping (Classen *et al.*, 1998). Furthermore, motor maps often show several local maxima contributing to the position of the COG. In these cases it remains unclear whether the local maxima result simply from noise or from several distinct representations. In general, inferring a cortical target site from the motor map is always subject to a certain amount of uncertainty and must be regarded with caution. Correlation studies comparing the COGs of maps obtained by TMS and functional imaging methods support this view (Wassermann *et al.*, 1996; Bastings *et al.*, 1998; Rossini *et al.*, 1998; Terao *et al.*, 1998). They consistently report a deviation of the COGs in a range of 10–20 mm.



1053-8119/02 $35.00

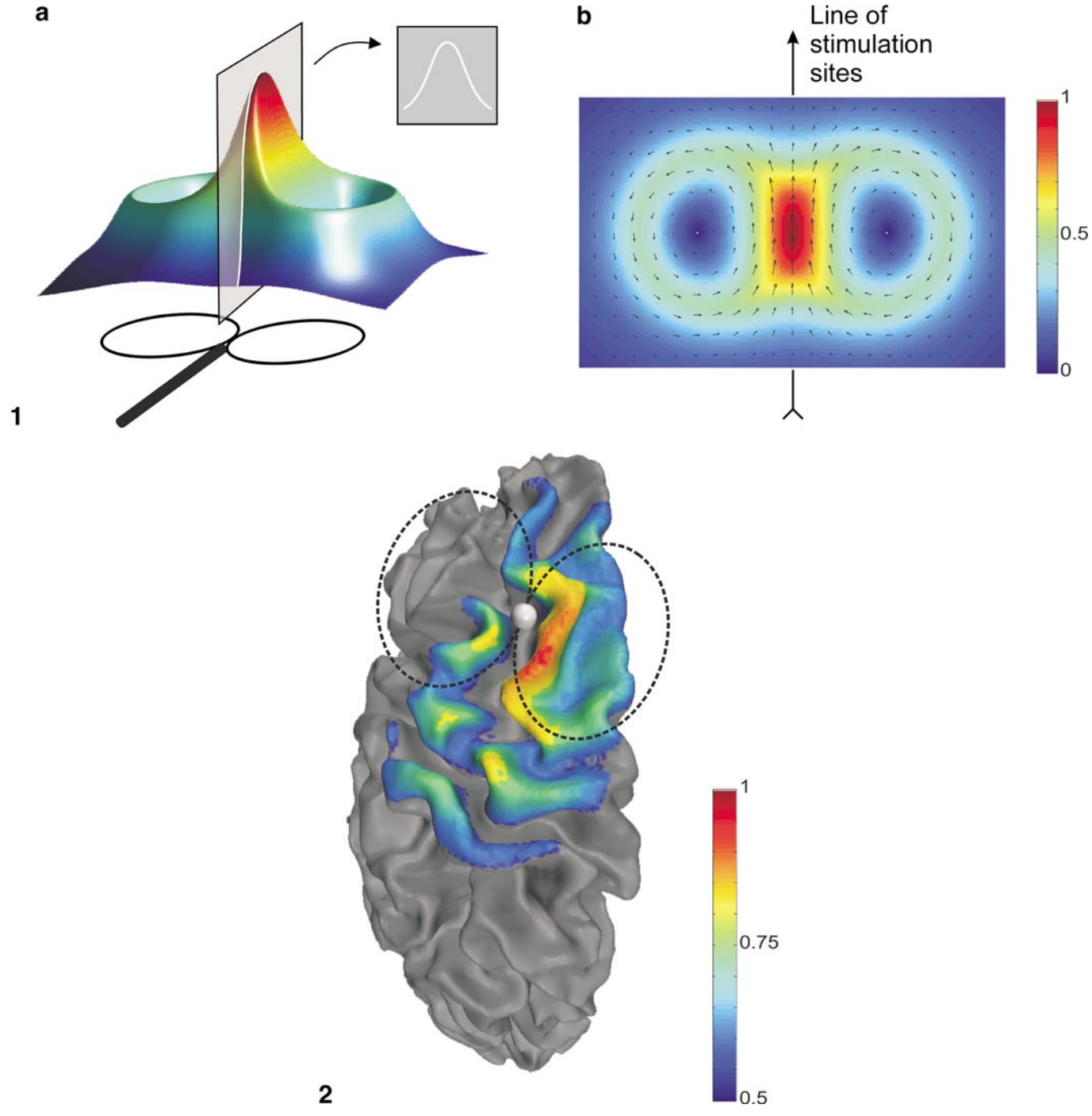


**FIG. 1.** (a) Electrical field strength calculated on a plane 1 cm above the coil plane. The field strength is coded as both color and height. The inset depicts the bell-shaped form of the field strength along the axis parallel to the coil handle. (b) The 2D plot of the electrical field on the same plane. The strength is color coded. The arrows indicate the direction of the induced currents. For the same current direction to be maintained over various target sites, theses sites have to lie on the indicated line.

**FIG. 2.** Distribution of the electric field on an individual cortical surface, as rendered from anatomical MR data. The field distribution is calculated on the basis of the sphere head model for the indicated coil position, normalized to the maximal field strength reached on the cortical surface and coded as color. Notice the rapid decrease in field strength in the sulci.

The motor maps described so far are restricted to purely physiological measurements. They do not take into account the physical field distribution of the stimulation coil. Whereas the magnetic field is easy to calculate by means of the Biot–Savart law, the induced electric field causing neural stimulation is much more

difficult to characterize. It depends on the complex conductivity profile of the head. The currently available models assume the head to be a perfect sphere in order to reduce complexity, thereby rendering a mathematical solution of the electric field distribution feasible (Sarvas, 1987; Roth *et al.*, 1991; Eaton, 1992; Ravazzani *et al.*, 1996). Within a purely physical framework, such sphere models have been used to compare the induced electric fields of different TMS coil geometries (Fig. 1). However, a direct link between predicted fields and individual physiological data is difficult to establish. In principle, the sphere models can be used to calculate the electric field distribution on an individual cortical surface. Unfortunately, these distributions do not provide any information about the site and size of the stimulated cortex. For example, at the coil position depicted in Fig. 2, a motor response can be evoked with high stimulator output intensity. Nevertheless, the maximum of the induced field resides within the prefrontal cortex and not within the primary motor cortex.

In this paper, we present a method linking physiological measurements with physical models. Applied to the motor system, it allows us to directly calculate the *cortical* stimulation site as well as the individual cortical stimulation threshold.

Our strategy is based upon three assumptions: (i) Cortical tissue is stimulated when a certain threshold of field strength is reached. (ii) The physiological effect (e.g., the motor response) originates from a single, small cortical target area. (iii) Sphere models describe the real electric field induced in the head with sufficient accuracy. For the motor system, the first two assumptions have been shown to be plausible. The validity of the third assumption can be derived from MEG studies.

(i) The relevant parameter determining the excitation of cortical tissue is thought to be the induced electric field strength (Amassian *et al.*, 1992; Ilmoniemi *et al.*, 1999). Additionally, thresholds have been reproducibly determined (Kammer *et al.*, 2001; Stewart *et al.*, 2001). Taken together, this suggests that cortical tissue is excited by TMS only if the induced field strength exceeds a certain threshold. This is possible only if the direction of the induced electric field is kept constant, since stimulation of the motor cortex with different current directions results in different responses (Brasil-Neto *et al.*, 1992; Mills *et al.*, 1992; Pascual-Leone *et al.*, 1994; Kammer *et al.*, 2001).

(ii) In the precentral gyrus, M1, the cortical representation of different muscles is known to be organized in a somatotopic manner (Penfield and Rasmussen, 1950). Although recent data suggest that a huge overlap between representations of different muscles exists, the neuronal representations for a given muscle are distributed rather narrowly (e.g., thenar representation $< 5 \times 4$ mm, Schieber, 2001). Given the macroscopic resolution of TMS, this can still be considered a dot-shaped representation. This view is supported by a TMS study investigating input–output functions at different coil positions over the motor cortex (Thickbroom *et al.*, 1998). By and large, all input–output functions of motor responses have a similar shape and steepness, independent of the actual stimulation site. They are merely shifted by a certain value of stimulation intensity which increases monotonically with the distance from the optimal stimulation site.

(iii) In magnetoencephalography (MEG), sphere models have been compared with more complex finite-element models of the head. It could be shown that sphere models accurately account for the magnetic field distribution of a given dipole, with the exception of deep frontal and frontoparietal areas (Hämäläinen and Sarvas, 1989). As the reciprocity theorem holds for MEG and TMS, these results can be adopted for TMS (Ravazzani *et al.*, 1996).

In combination, the three assumptions allow to directly determine the cortical stimulation site using the strategy depicted in the following.

Think of an electrode being placed in the cortical target area representing the target muscle. At several coil positions, TMS output intensity is adjusted to induce a motor response of a certain constant strength. Given the assumptions (i) and (ii), the electrode will always record the same electric field strength, regardless of the coil position. In contrast, the electrode will record field strengths varying with coil position when it is displaced from the target area. Therefore, the cortical target area is the only position on the cortex where the same electric field strength is always induced for a constant motor response, regardless of the stimulation site.

Using the TMS output intensities derived by this method, the sphere model (assumption (iii)) can be used to calculate the electric field strength on the cortex without implanting an electrode (Fig. 2). The cortical target site is then identified as that position where the calculated field strength is identical for all coil positions. In the real experiment, the determined TMS output intensities are influenced by noise. In this case, the target area is the cortical position at which the field strengths over all coil positions are most similar to each other. Mathematically speaking, this is the point at which the variance of the field strengths over all stimulation sites is minimal.

Assumption (i) holds only if current directions are kept as constant as possible in the cortical target area. This can be achieved by placing the stimulation sites on a line running approximately over this area, with the coil handle kept parallel to that line. Under such conditions, the target area “resides” on the field distribution curve at the sagittal section, as shown in the

inset of Fig. 1a. In addition, it can be seen from Fig. 1b that current direction is kept constant in two dimensions under such stimulation conditions. As the spherical boundary of the head suppresses radial components of the electric field this also applies to the third dimension (Sarvas, 1987).

The general idea of the experiment is depicted in Fig. 3, showing stimulator output intensities for three stimulation sites along the line running over the target area (Fig. 3a). These intensities can be used to calculate electric field distributions by means of the sphere model (Fig. 3b). The field distribution curves intersect at exactly one point which coincides with the cortical representation of the target muscle.

In the actual experiment, compound muscle action potential (CMAP) amplitudes over the whole range of stimulator output intensities (input–output function, Devanne *et al.*, 1997; Thickbroom *et al.*, 1998) were measured at several coil positions along the line over the target area. We recorded CMAP amplitudes in the right abductor pollicis brevis muscle (APB). Its cortical representation in the precentral sulcus (Levy *et al.*, 1991; Wassermann *et al.*, 1996; Krings *et al.*, 1997; Classen *et al.*, 1998) constitutes the target area in the experiment. The approximate position was determined by searching for the "hot spot" with the maximal CMAP amplitude response (Classen *et al.*, 1998). The line on which the measurements were performed was oriented perpendicular to the main axis of the central sulcus, as individually determined for each subject by means of online tracking and visualization of coil positions in the individual anatomical magnetic resonance images (MRI) (Kammer *et al.*, 2001). The distribution of the electric field strength on the cortex was calculated for each coil position using the half-maximal response strength measured by means of the input–output function (cf. Fig. 2). The cortical site was determined as the voxels with minimal variance of field strengths over all coil positions.

While the three assumptions are plausible, they differ in their empirical support. As all the three assumptions must be met to obtain significant results with the proposed strategy, they act as hypotheses that are directly tested by our approach.

## METHODS

### Participants

Four subjects (age 25–38 years, three male, one female) were investigated. They were all in good health and had no history of neurological disorders. The experiments were approved by the local internal review board of the Medical Faculty, University of Tübingen, and written informed consent was obtained. All subjects were right-handed as assessed by the Edinburgh inventory (Oldfield, 1971).

### MR Imaging

High-resolution MR scans were obtained with a 1.5-T Magnetom (Siemens, Erlangen, Germany) using a T1-weighted flash sequence. For each subject, the surface of the head was reconstructed by means of Brain Voyager 4.4 (Brain Innovation B.V., Maastricht, The Netherlands). Additionally, the border between the gray and white matter of the left hemisphere was segmented and rendered.

### Experimental Setup

Stimulation was performed with a Magstim 200 stimulator (Whitland, Dyfed, UK) and a standard figure-of-eight coil. The coil was held tangentially to the skull and the coil handle was oriented perpendicular to the central sulcus using the online visualization function of the positioning device.

CMAP was recorded from the right abductor pollicis brevis muscle and peak-to-peak amplitude was assessed. Subjects were given auditory and visual feedback to ensure constant low-level contraction of the target muscle (mean CMAP about 100 $\mu$V) (Hess *et al.*, 1987).

The position of the coil relative to the subject's head was monitored online by a positioning device based on two mechanical digitizing arms (Kammer *et al.*, 2001). The coil position in 6 *df* was stored at each TMS stimulus together with the CMAP amplitude.

### Determination of the Line of Measurement

Prior to the experiment, the position and orientation of the line of measurement were determined. First, using a suprathreshold TMS pulse the rough position of the maximal CMAP response ("hot spot") was determined and the active motor threshold was measured. Second, the coil was shifted laterally and medially parallel to the central sulcus in steps of 1 cm, in order to specify the position of the hot spot more precisely. At each position, four stimuli were applied with an intensity of 120% of the motor threshold. The mean value of the recorded CMAP was calculated. This resulted in an inverted U-shaped curve of mean CMAP values along the central sulcus. The line of measurement was determined to be perpendicular to the central sulcus and to lead through the maximum of the inverted U. In all subjects, this line also crossed the lateral part of the hand knob.

### Measurement of the Input–Output Functions and Sigmoidal Fit

The coil was moved in steps of approximately 1 cm along the line perpendicular to the central sulcus. This was repeated until anterior or posterior positions were reached at which CMAP could not be obtained even at 100% of stimulator output. For each coil position, stim-

uli were delivered at continuous levels of stimulator output intensity starting at 20% and increasing in steps of 10% while subjects maintained a low-level preinnervation of the target muscle (Thickbroom *et al.*, 1998). We chose this low-level preinnervation for two reasons. First, compared to the relaxed state the input–output functions are shifted to lower stimulator output intensities (Devanne *et al.*, 1997). This made it possible to obtain responses from a larger range of coil positions. And second, a good reproducibility of the input–output function has been demonstrated with low-level preinnervation (Devanne *et al.*, 1997). The stimulation frequency was restricted to a maximum of 0.2 Hz. Four stimuli were applied at each level and a mean CMAP amplitude was calculated. The measurement was terminated when the CMAP amplitude had saturated or when 100% of stimulator output had been reached.

Sigmoidal curves were fitted to the input–output functions using the Boltzmann equation

$$y = \frac{A_1 - A_2}{1 + e^{(x - x_0)/dx}} + A_2,$$

with $A_1$ and $A_2$ as the lower and upper boundaries, $x_0$ as the half-maximal value, and $(A_2 - A_1)/4dx$ as the slope at $x_0$. Since the gradient of the sigmoidal function is maximal at $x_0$ and therefore the estimation is most accurate, the stimulator output intensities for half-maximal CMAP values were used for the calculation of the electric field.

A constant value of the upper boundary $A_2$ was used to ensure a realistic shape of the sigmoidal functions at anterior and posterior positions at which the CMAP amplitude did not saturate even at 100% of stimulator output intensity. The mean value of all CMAP amplitudes which reached at least 90% of the maximal CMAP amplitude was calculated and used as $A_2$.

### Calculation of the Variance of Electric Field Strength

The sphere dipole model (Ravazzani *et al.*, 1996) was implemented in MATLAB 6.0 (The Mathworks Inc., Natick, MA). The dipole model of the coil was created using X-ray pictures and the approach explained in the same paper. A detailed specification of the coil model can be found in Appendix A. The structural MR scan and the segmented and rendered left hemisphere and the coil positions were read using custom-made software. The sphere of the model was visualized as circles on the sagittal, coronal, and horizontal planes of the structural MR. Within the range of the coil positions it was manually fitted to the inner surface of the skull (Ilmoniemi *et al.*, 1999).

We then calculated the electric field strength in each voxel of the rendered left hemisphere for each coil position. More precisely, the field strength for the peak value of $dI/dt$ at the start of the TMS pulse was calculated. Equation 12 of Ilmoniemi *et al.* (1999),

$$\left.\frac{dI}{dt}\right|_{t=0} = \frac{\sqrt{2W}}{\sqrt{CL}} = \frac{\sqrt{2 \cdot 720\ J}}{\sqrt{185\ \mu F \cdot 16.35\ \mu H}} = 171 \cdot 10^6 \frac{A}{s},$$

was employed to determine the maximal value of $dI/dt$ at a stimulator output intensity of 100% (conductance of the coil $L = 16.35\ \mu$H, capacity of the stimulator $C = 185\ \mu$F, maximal energy stored in the capacity $W = 720$ J, according to the specification of the stimulator). The determined value was used to convert the stimulator output intensities for half-maximal CMAP responses into values of $dI/dt$ by means of the rule of proportion.

The variance of the induced field strengths of the different coil positions was calculated for each voxel. The position of the voxel with the minimal variance and the positions of the voxels with a variance $<7\%$ were determined. The result was visualized by means of Brain Voyager.

**TABLE 1**

Calculated Electric Field Strength in the Cortical Representation of the Target Muscle for Half-Maximal CMAP Responses

| Subject | Half-maximal CMAP amplitude (mV) | Minimal variance of induced field strength at the cortical surface (%) | Electric field strength (voxel of minimal variance) (V/m) |
|---|---|---|---|
| AT | 3.05 | 4.4 | 79.5 ± 3.4 |
| MV | 3.80 | 3.2 | 70.1 ± 2.2 |
| SaBe | 4.87 | 4.2 | 100.5 ± 4.2 |
| TK | 2.76 | 5.1 | 93.2 ± 4.8 |

## RESULTS

Input–output functions were measured at 9 to 13 different coil positions along the line individually determined for each of the four subjects. The positions were chosen at roughly equidistant intervals of 1 cm anterior and posterior to the hot spot. In Fig. 4a, input–output functions are depicted from three different positions in one subject. Sigmoidal fits allow us to determine the stimulator output intensities for half-maximal CMAP responses, which were taken as threshold values for the calculation of the electric field (Table 1). We chose this half-maximal CMAP value as the threshold because the slope of the sigmoidal function is maximal at this point and therefore the estima-

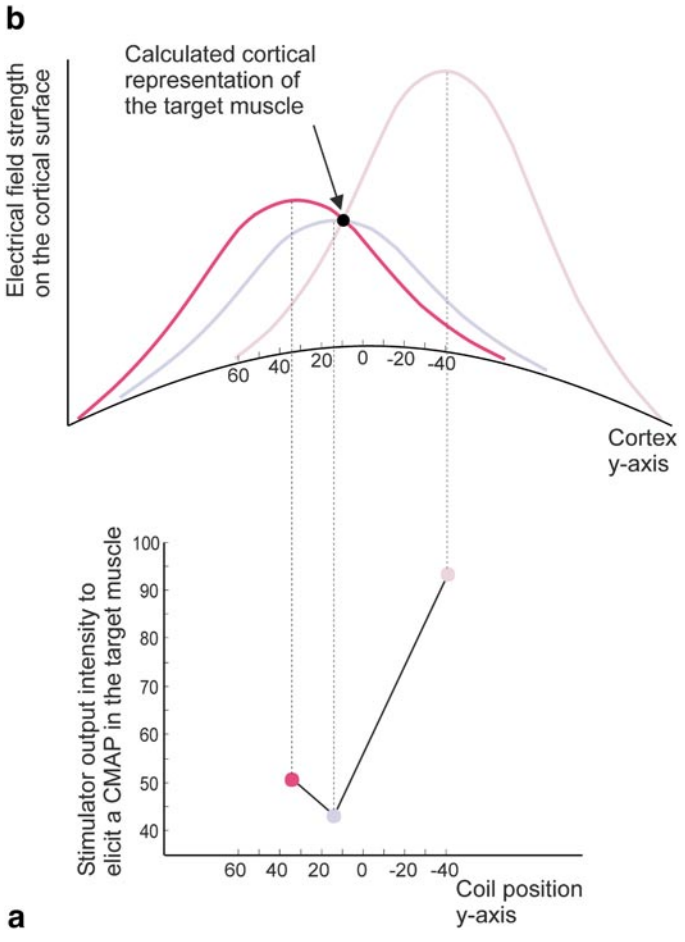


**FIG. 3.** Schematic illustration of the hypothesis underlying the experiment. (a) The minimal stimulator output intensity required to elicit a response in the target muscle is shown for three stimulation sites. The abscissa gives the coordinate of the coil position along the anterioposterior direction (*y* axis, 0 is arbitrarily chosen, cf. Fig. 4b), which is the main direction of coil movement at the skull. (b) Field distributions in the anterioposterior direction for the three coil positions shown in (a). As the coil handle is orientated in the same direction, the induced field is bell shaped (see inset of Fig. 1a). The maxima of the fields depicted on the ordinate depend linearly on the stimulator output intensities shown in (a). Assuming that the threshold remains constant in a circumscribed cortical region, this region will be stimulated at any position of the coil, but stimulus intensity has to be adjusted so that the local field strength exceeds the threshold in this region. The target region can be calculated as the region in which the electric field strength is the same for all coil positions (section point of the three field distribution curves).

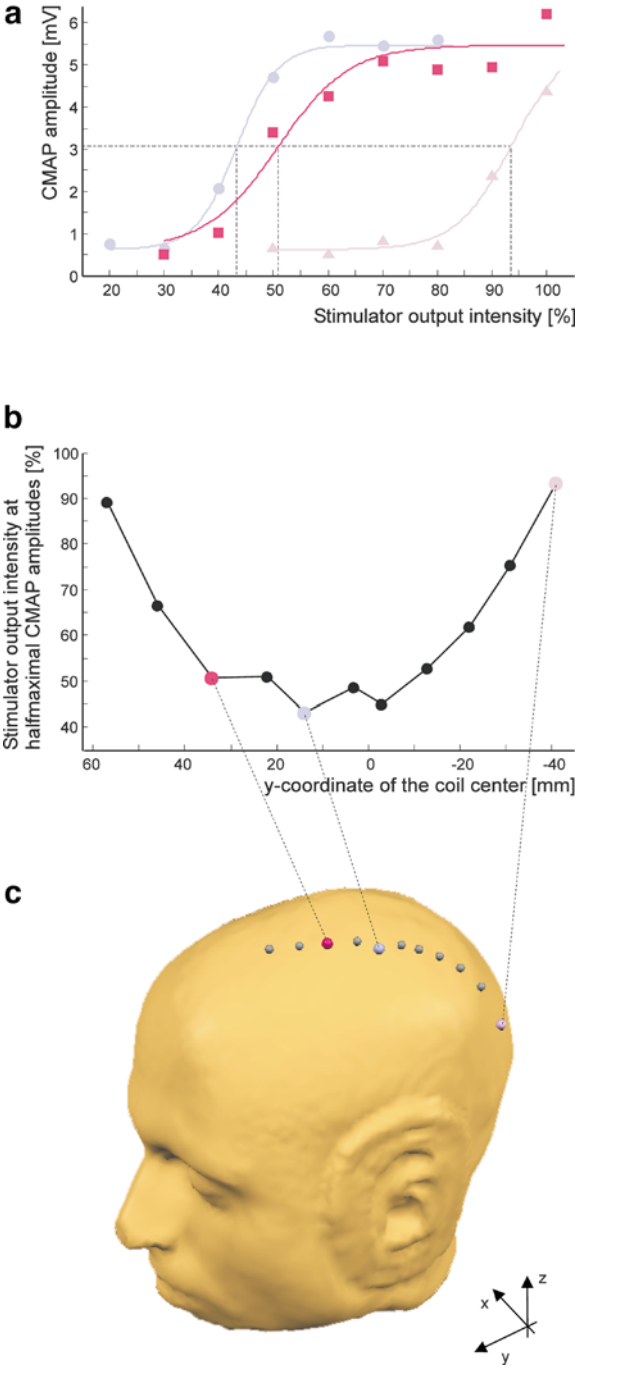


**FIG. 4.** Motor responses depend upon TMS intensities at different stimulation sites. (a) Input–output functions for three different stimulation sites (subject AT) coded in blue, red, and purple. The half-maximal amplitudes were derived with sigmoidal fits as the most accurate estimate of response strength to TMS. (b) The position-dependent TMS intensities (for half-maximal response) form a U-shaped function (middle) along the *y* axis of the head coordinate system. Zero indicates the origin of the head coordinate system and is not related to the measured data. Notice that the ordinate corresponds to the abscissa in (a). (c) The 3D model of the individual skull as derived from the anatomical MR scan. The spheres depict all coil positions at which input–output functions have been measured.

tion is most accurate. Figure 4b shows the stimulator output intensities for these half-maximal CMAP responses as a function of coil position. Stimulator output intensities for the half-maximal CMAP responses of all 4 subjects are shown in Fig. 5. Minor deviations from an ideal U shape occurred in three of the four subjects at one or two coil positions.

In each subject the distribution of the electric field was calculated across all the voxels in the individual cortical surface for each individual coil position used

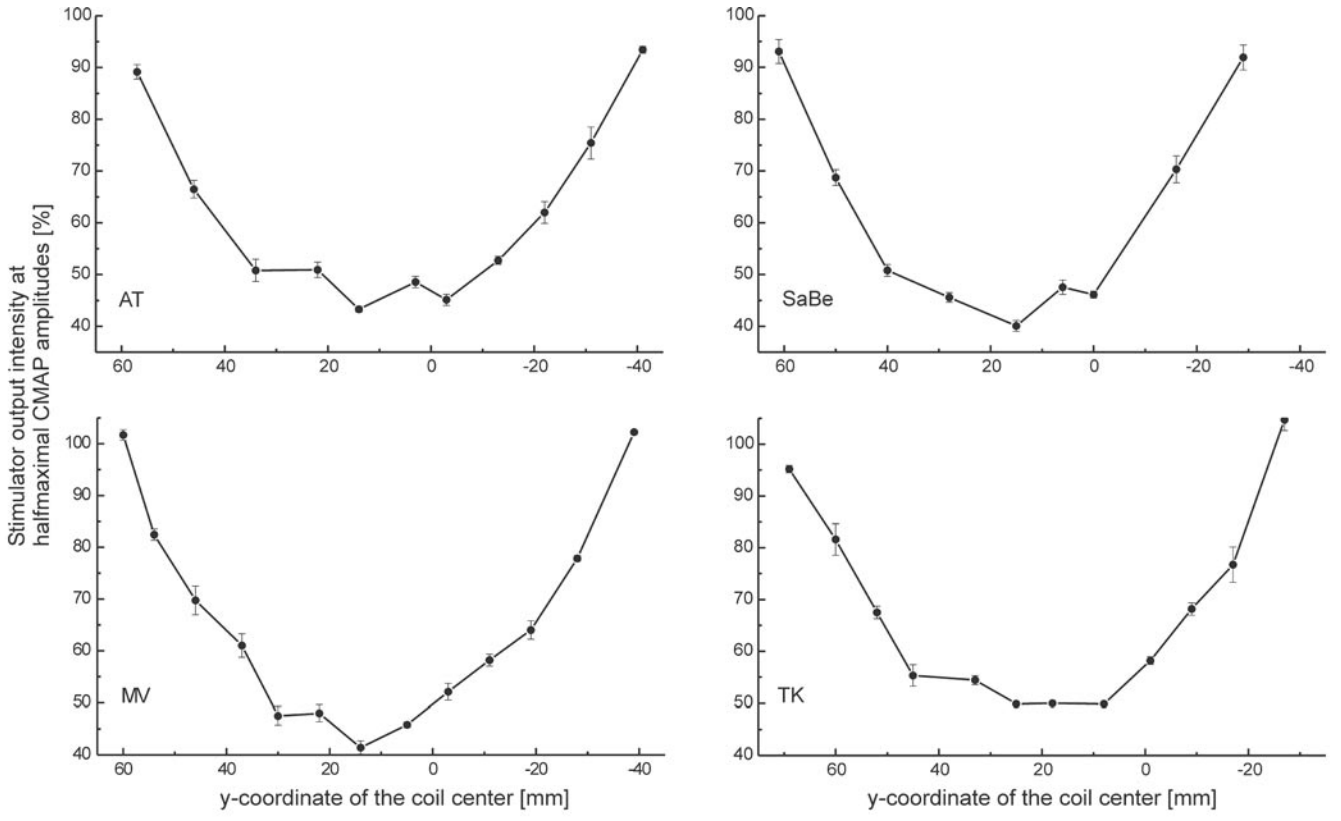


5

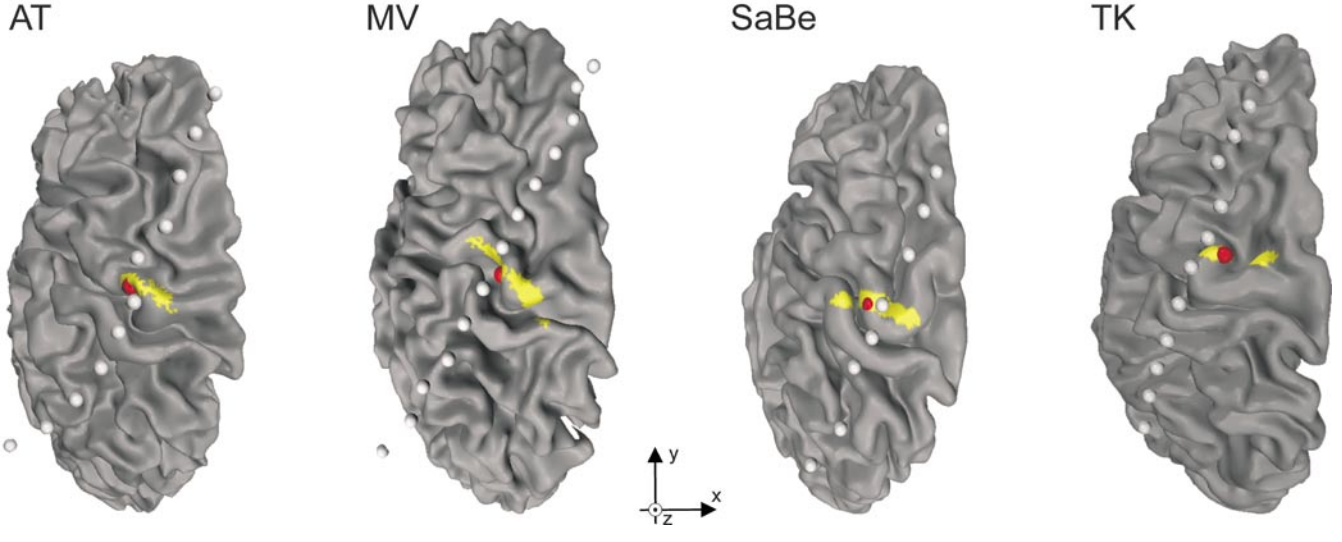


6

**FIG. 5.** Stimulator output intensities of the half-maximal responses as a function of the coil position. Individual data from all four subjects are shown. On the abscissa the *y* coordinate of the head coordinate system is given. Zero indicates the origin of the head coordinate system and is not related to the measured data. The stimulator output intensities (in percentages of maximal output) are taken from the sigmoidal fits of the input–output functions measured in each subject.

**FIG. 6.** Area of calculated minimal variance (<7%; yellow) on four individual brains. The point of minimal variance in each case is indicated by a small red sphere. The minimal variance is given in Table 1. Light gray spheres show the coil positions used.

(Fig. 2). Absolute values for the electric field strength were calculated using the stimulator output intensities of the half-maximal CMAPs. In each voxel of the cortical surface the field strength values of the different coil positions were compared with each other by calculating the variance. The minimal variance ranged between 3.2 and 5.1% in the four subjects (Table 1), with a mean value of 4.2 ± 0.8%. In Fig. 6 the voxel with the minimal variance is depicted as a red sphere on the individual cortex for each subject. In all cases this

voxel was situated at the lateral part of the hand knob. All voxels on the cortex with a variance below 7% (arbitrarily chosen to demonstrate the distribution of the voxels) are indicated in yellow in Fig. 6. They form a narrow stripe perpendicular to the line of coil positions crossing the hand knob. In subject TK the line was disrupted in the junction zone of the precentral and the superior frontal sulcus.

The absolute field strength values required for half-maximal CMAP amplitudes vary from one subject to the next, but always lie in the range of 70 to 100 V/m (Table 1).

### Comparison with Model Calculations

Variance model calculations were performed in order to account for the remaining 4.2% (cf. Appendix B). The main results of the calculations are depicted in Fig. 7. If the remaining variance were due to systematic over- or underestimation of the field distribution or to more than one target area, the result would be a systematic variation of the field strength (either U shaped or inverted U shaped) induced in the voxel of minimal variance (Fig. 7a). As no such systematic variations were measured (Fig. 7b), the observed remaining variance can be attributed to noise.

Finally, in a model calculation the result of the minimal variance method assuming the maximal field strength to be the relevant stimulation parameter (Fig. 8a) is contrasted with a calculation considering the spatial derivative of the electric field strength as the relevant parameter (Fig. 8b). Using a U-shaped function of half-maximal CMAP responses in dependence on the coil positions (similar to the measured curves depicted in Fig. 5) and considering the electric field strength as a relevant parameter results in a minimal variance of 4.2% (Fig. 8a). However, the same U-shaped function results in a minimal variance of 68% when the calculation is repeated utilizing the spatial derivative (Fig. 8b).

## DISCUSSION

Our results show that physical field models and physiological measurements can be successfully combined in order to determine the cortical stimulation site of TMS. We were able to identify, in each of the four subjects, an area in the motor cortex where the variance of the calculated field strengths was 5.1% or less (mean value 4.2 $\pm$ 0.8%). The solutions are highly plausible, as can be shown by data from anatomical studies and from model calculations.

### Anatomically Correct Position of the Identified Area

The voxels with minimal variance were located within an anatomical structure that was previously described as an invariable landmark for the representation of hand muscles, the so-called hand knob (Yousry *et al.*, 1997). Within the hand knob a somatotopic map exists, with representations of the muscles of the little finger located medially and representations of the muscles of the index finger and thumb located laterally (Beisteiner *et al.*, 2001). In all subjects the voxel with minimal variance was located on the lateral end of the hand knob, in accordance with the known somatotopic map and indicating that the identified target areas reside at anatomically correct positions.

### Validity of the Initial Assumptions

Our results are in accordance with the three crucial assumptions of the experiment, i.e., the concept of a stimulation threshold, the sufficient accuracy of the sphere model, and the dot-shaped cortical target area. However, as pointed out in the Introduction, the result of a low minimal variance can be obtained only if all three assumptions are met in conjunction. This is demonstrated quantitatively by the model calculations in Appendix B. In these simulations, the impact of violations of the three assumptions on the result is examined. The violation of assumption (ii), i.e., of the dot-shaped representation of a muscle, would result in a systematic deviation of the measured minimal variance in dependence on the coil position (Fig. 7a). No such systematic deviation was observed, but instead a noise-like distribution (Fig. 7b), thus validating assumption (ii). The same discrepancy between expected systematic deviation and measured noise validates assumption (iii), i.e., the accuracy of the calculated electric field of the stimulation coil (Figs. 7a and 7b). Finally, with regard to assumption (i), we found the alternative, i.e., the spatial derivative of the electric field as the relevant feature determining the cortical stimulation site (instead of the electric field strength itself), to yield 68% of minimal variance in contrast to the obtained value of 4.2% (Fig. 8). Taken together, the simulations reveal that the chosen experimental strategy does indeed react quite sensitively to even minor changes from the initial set of assumptions. This renders the production of our result by any other set of assumptions highly unlikely, thereby validating the proposed set of assumptions.

In each subject the voxels with a variance below 7% formed a narrow stripe perpendicular to the line of coil positions. This indicates that the resolution of our method is high in the direction of the line chosen, but lower in the perpendicular direction. As the goal of our experiment was to test the general feasibility of the minimal variance strategy, we restricted our measurements to one line of coil positions. This experimental strategy can be augmented by measuring a second line oriented perpendicular to the first one. By calculating of the field variances for the two measured lines independently of each other, we should be able to find a

small intersection region of the two 7% stripes, thereby narrowing down the cortical target even further.

### Relation to Motor Maps

In classical motor mapping, the probable stimulation site is determined by calculating the COG (Brasil-Neto *et al.*, 1992; Wassermann *et al.*, 1992, 1996; Wilson *et al.*, 1993; Classen *et al.*, 1998). Implicit assumptions made with that procedure include the existence of a single cortical target area and a monotonous dependence of the muscle response on the field strength induced in that area. However, during motormapping it is frequently the case that one is observing not only a single maximum of activation but also other maxima in the neighborhood (Classen *et al.*, 1998).

The crucial question is whether the additional maxima are merely noise or result from more than one distinct target area. The classical mapping procedure cannot resolve this problem because of its inherent limitations. Furthermore, classical motor mapping does not permit an assessment of the extension of the cortical representation (Classen *et al.*, 1998).

Our data show that in fact a single target area exists which is much smaller than the size of the induced fields. Inside of this area the muscle response depends only on the locally induced electric field strength, given a constancy of current direction. Both implicit assumptions of the calculation of a COG are therefore validated. In the classical motor mapping procedure, current directions are not optimized and vary with the coil position, resulting in deformed maps.

Additional maxima in a motor map correspond to minor deviations from the ideal U-shaped function observed in our study (Fig. 5). A calculation of field variance based only on sites in the middle part of the U-shaped distribution pattern cannot distinguish between a distributed motor representation and noise in a small cortical target area. Only the full range of the U-shaped function reliably identifies a single small target area when the method of minimal variance is used. Thus the center of gravity calculated by the classical motor map approach may deviate from a position above the single cortical target area, because additional spurious maxima are contributing to the coordinates of the center.

Recently, a more precise method of determining the site of stimulation on the cortex by deconvolving a TMS map was published (Bohning *et al.*, 2001). This deconvolution method suffers from the same weaknesses as the maps it rests upon. Additional activations in the map are transformed into distinct activation centers on the cortex, although our results suggest that these additional centers are likely to result from noise. This may be inferred from Fig. 4 of the deconvolution paper (Bohning *et al.*, 2001), which shows several additional activation foci at a stimulator energy level of 120% of the motor threshold. However, when the stimulator energy level was increased to 125% these additional foci were no longer present and only one center remained in the deconvolved map. This result is most likely caused by a disproportionately higher noise level at lower stimulator energy levels.

It is not possible to monitor the correctness and quality of the solution using the deconvolution method. In contrast, our method allows us to assess the quality on the basis of the minimal variance. Furthermore, the curve representing the dependency of the electric field strength in the voxel of minimal variance on the coil position (Fig. 7b) can be checked for systematic fractions, allowing us to estimate the maximal distance of distinct target areas or the maximal size of a distributed area.

### Individual Differences in Cortical Thresholds

One advantage of the approach taken here is that it provides absolute field strengths for suprathreshold stimulation on the cortical surface. As shown in Table 1, field strength varies considerably across subjects. Motor threshold measurements always show a large interindividual variability (Mills and Nithi, 1997; Kammer *et al.*, 2001). It has been proposed that a main source of this variability is the difference in the thickness of the skull. In two studies this link has been demonstrated, but the correlation of skull thickness and motor threshold was weak (Kozel *et al.*, 2000; McConnell *et al.*, 2001). This weak correlation can be explained by the variability of field strengths required for suprathreshold stimulation, as revealed by our method.

An alternative method of determining absolute field strength values has been reported (Epstein *et al.*, 1990). It is based on the comparison of motor thresholds measured with two coils that differ in geometry and therefore have different field profiles with increasing distance to the coil plane. The values reported there (100–130 V/m) are 30% higher than our results but have the same between-subject variability. However, the 30% difference can be explained by the following methodical discrepancy. The higher values are based on measurements in the air using a rectangular search coil (Branston and Tofts, 1990). Field strengths of a figure-of-eight coil in the air have been calculated to be 32% higher than the strengths in a spherical conducting medium (Ravazzani *et al.*, 1996), which corresponds nicely to the difference between the values reported by Epstein *et al.* (1990) and our values.

According to a recent review (Ilmoniemi *et al.*, 1999), simplified sphere models can merely account for "gross features of the induced electric field" and therefore are only a spatially limited approximation of the effective field. In fact, it has been proposed that finite element models of head anatomy are needed to address the

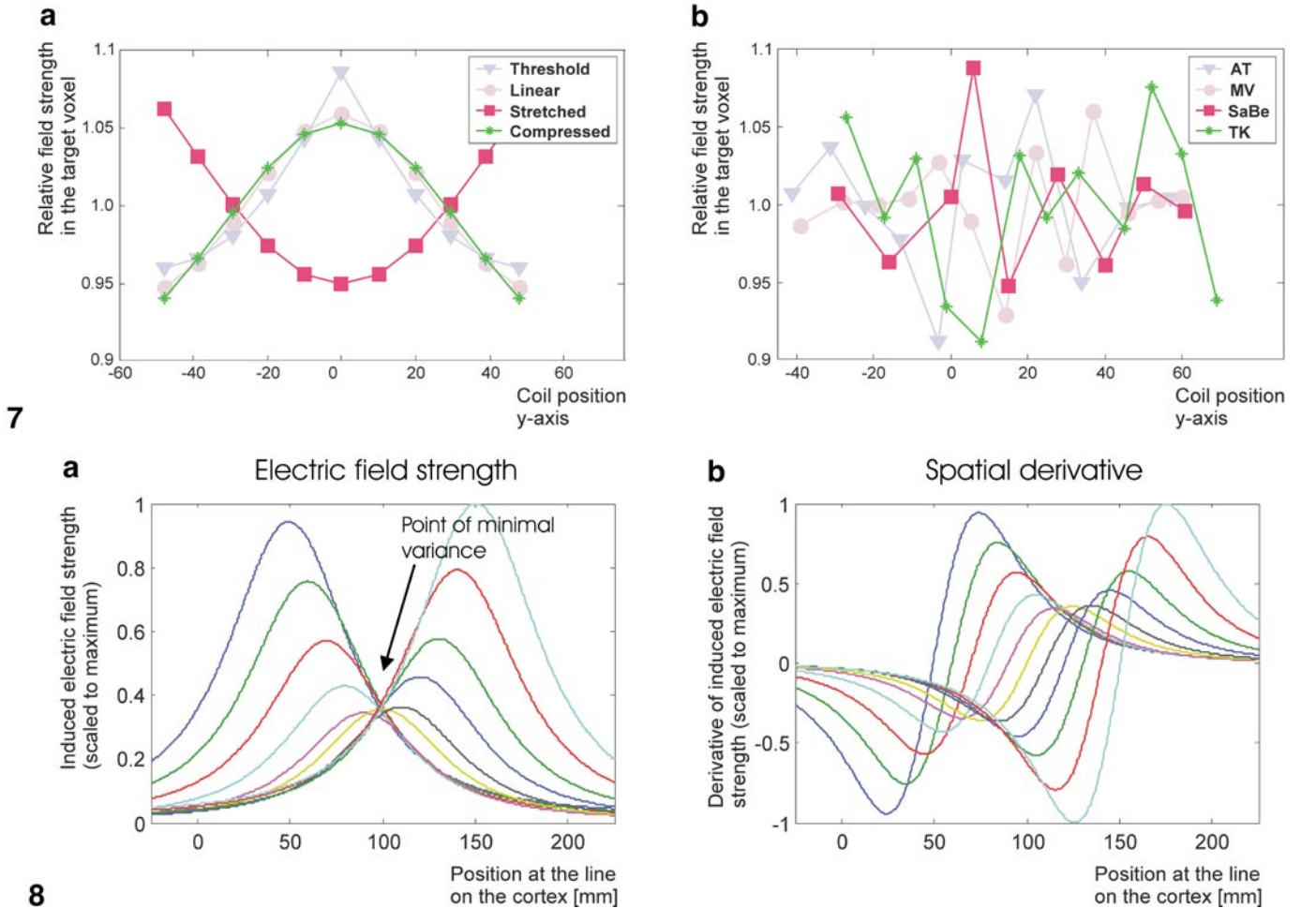


**FIG. 7.** Electric field strength in the voxel of minimal variance as a function of the coil position, normalized to the mean field strength over all stimulation sites. (a) Simulation results for four different systematic deviations: green, field prediction too narrow (coil size shrunk to 87%); red, field prediction too expansive (coil size stretched to 116%); blue, two distinct target areas (distance 8 mm) characterized by a step function; purple, two distinct target areas (distance 22 mm) characterized by a linear input–output function. All calculations result in a variance of 4.2% in the target voxel. Eleven stimulation sites spaced 1 cm apart on a circular line (9.5-cm radius) placed over the target voxel (8-cm radius) are simulated. The electric field strength in the target voxel induced by the coil position closest to it corresponds to 40% stimulator output intensity. This field strength is the threshold of the step functions and the input value for a half-maximal output of the linear input–output functions. The two distinct target areas were placed symmetrically around the voxel of minimal variance on a circular line (8-cm radius) beneath the line of coil positions. (b) Individual data of the four subjects measured. The absence of any discernible pattern in these curves indicates that noise is the main source of the variance.

**FIG. 8.** Comparison of electric field strength vs the spatial derivative of the induced field. (a) For all coil positions, the electric field strength on a line beneath the line of coil positions and lying on the cortical surface (approximated by a hemisphere with a radius of 8 cm, origin arbitrarily chosen) is depicted (scaled to the maximum). The curves can be seen to intersect roughly in the center of the graph at 100 mm. At this point, the variance is 4.2% in the model calculation. (b) The derivative of the electric field along the chosen line is calculated for all coil positions. The curves have no common intersection point. The points of minimal variance reside at 48 and 152 mm on the graph. The minimal variance at these positions is 68%.

complex consequences of conductance inhomogeneities (Roth *et al.*, 1991; Liu and Ueno, 2000). In contrast to this cautious view, we show that with respect to superficial cortical areas such as the motor cortex, the sphere model is sufficiently accurate to provide quantitative accounts of field strength.

In conclusion, our results provide an important link between the physical sphere model of electromagnetic fields applied to the brain and its physiological motor responses to TMS. Besides the implications for TMS the validation of the sphere model supports its use within the context of MEG.

## APPENDIX A

### Dipole Model of the Magstim Figure-of-Eight Coil

A photo and two X-ray pictures of the Magstim figure-of-eight coil are shown in Fig. A1. It consists of two wings with nine wire loops each. The outer and inner

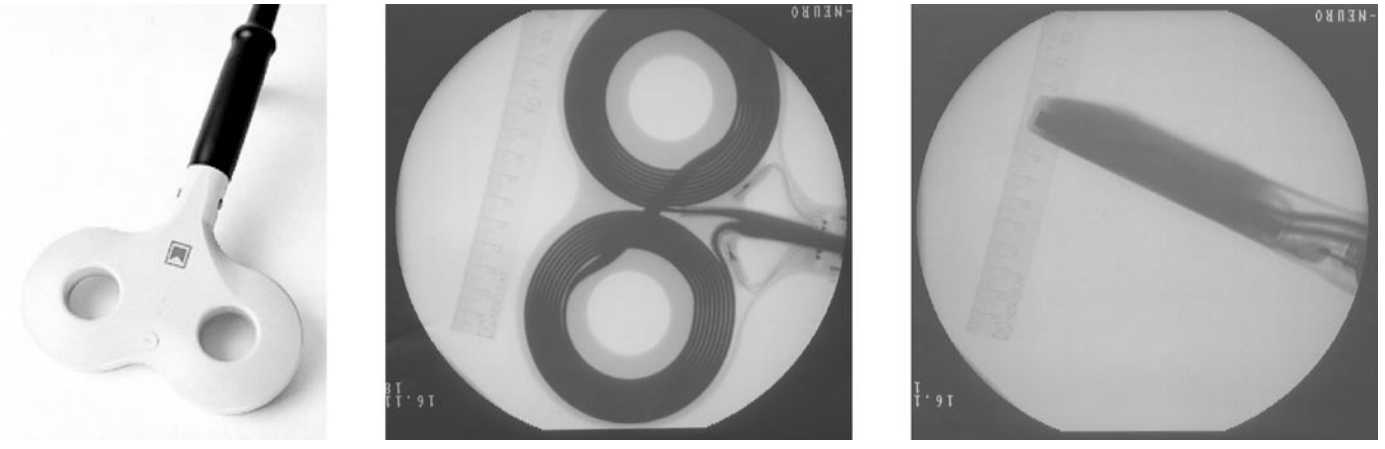

**FIG. A1.** Photo and X-ray pictures of the Magstim figure-of-eight coil.

radii of the loops are 4.4 and 2.6 cm, respectively. The wire is 1 mm wide and has a height of 7 mm. The thickness of the plastic chassis is 3 mm on the side attached to the head.

A method of approximating a coil using magnetic dipoles was described by Ravazzani *et al.* (1996). Briefly, the coil area is divided into subregions and the dipoles are placed perpendicular to the coil area in the centers of the subsurfaces. The dipoles are weighted by the coil current and the areas of the subregions. In contrast to the idealized figure-of-eight coil consisting of two loops of infinitely thin wire as modeled by Ravazzani *et al.* (1996), the Magstim coil has several loops in each wing and a wire 7 mm high.

This was taken into account when modeling the coil as follows: The dipoles were weighted by the area of the subregion and the amount of current circling around them. A dipole in the middle of a wing is surrounded by nine loops and was therefore weighted by nine times the coil current. A dipole at the outer loop is surrounded by only one loop and consequently weighted by once the coil current. To summarize, the length of a dipole was determined by the area of the subsurface and $n$ times the coil current, whereby $n$ represents the number of loops surrounding the dipole.

In a first step, each wing of the coil was modeled as a circular disk and divided into 16 rings. Each ring was further divided into elements, as shown in Fig. A2. The inner and outer radii of the rings, the number of elements of each ring, and the number of surrounding loops can be found in Table A1.

To account for the height of the wire and the thickness of the plastic chassis, the circular disks were then divided into three planes each, which were shifted 4.2, 6.5, and 8.8 mm in the negative Z direction (see Fig. A3). Consequently, a plane carries one third of the current and all dipoles were weighted by a factor of one third. The current counterrotates in the two wings. The direction of the dipoles in one wing is therefore antiparallel to that of the dipoles in the other wing.

## APPENDIX B

We estimated the significance for the observed minimal variance using model calculations. The minimal variance can originate from noise, systematic deviations, or a combination of both. Systematic deviations are caused by a violation of assumptions (ii) or (iii), i.e., by the existence of a distributed cortical target area (or several distinct areas), or by inaccurate predictions of the induced electric field by the sphere model. In both cases, the effects on the induced electric field are depicted in the following.

### Systematic Errors Caused by the Sphere Model

The effects of systematic errors of the sphere model were estimated for two different predicted field distributions which were either too narrow or too wide. With a too-narrow field distribution (i.e., field decay modeled steeper than in reality), the electric field strength in the target area is progressively underestimated with increasing distance from the stimulation sites. In this case, plotting the calculated electric field strength in the voxel of minimal variance as a function of the coil position leads to an inverted U-shaped function (green

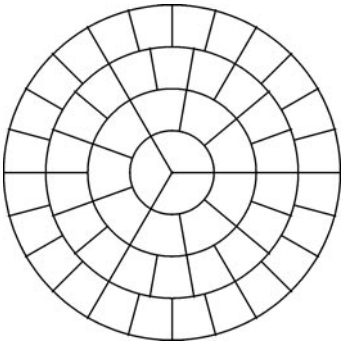

**FIG. A2.** Segmentation of a circular disk into elements of rings.

**TABLE A1**

Inner and Outer Radii of the Rings Representing One Wing, the Number of Elements per Ring, and the Number of Surrounding Loops

| | | | | | | | | | | | | | | | | |
|---|---|---|---|---|---|---|---|---|---|---|---|---|---|---|---|---|
| Inner radius (cm) | 0.0 | 0.3 | 0.7 | 1.1 | 1.5 | 1.9 | 2.3 | 2.6 | 2.8 | 3.0 | 3.2 | 3.4 | 3.6 | 3.8 | 4.0 | 4.2 |
| Outer radius (cm) | 0.3 | 0.7 | 1.1 | 1.5 | 1.9 | 2.3 | 2.6 | 2.8 | 3.0 | 3.2 | 3.4 | 3.6 | 3.8 | 4.0 | 4.2 | 4.4 |
| No. of elements | 3 | 9 | 12 | 16 | 20 | 24 | 28 | 30 | 32 | 34 | 36 | 38 | 40 | 42 | 44 | 44 |
| No. of surrounding loops | 9 | 9 | 9 | 9 | 9 | 9 | 9 | 9 | 8 | 7 | 6 | 5 | 4 | 3 | 2 | 1 |

line in Fig. 7a). A 4.2% of variance is reached with a compression of the coil geometry to 87% of its original size. Predicted field distributions which are too wide (i.e., field decay modeled flatter than in reality) result in an overestimation of the field strength in the target voxel induced at more distant coil positions (red U-shaped function in Fig. 7a). A 4.2% variance corresponds to a stretching of the coil to 116% of its original size.

### Effects of Two Isolated Cortical Areas

The effects of two isolated cortical areas contributing to the CMAP are modeled as follows. In general, two areas lead to a broadening of the U-shaped function defined by the half-maximal CMAP values in dependence on the coil position (Fig. 5). The broadened U-shaped function in turn leads to an underestimation of the field strength in the target voxel induced at more distant coil positions. In combining their activations and projecting to the hand muscle both the cortical and the subcortical areas contribute to the steepness of the sigmoidal input–output functions to an unknown degree. Two extrema are considered, corresponding to the upper and lower bounds of the steepness of the cortical input–output functions.

In one case, the cortical areas are modeled as step functions, being either zero or maximally activated and representing sigmoidal functions at maximal steepness. In this case, the subcortical areas cannot affect the slope of the input–output function, which allows us to replace them with a simple summation. The resulting function representing the field strength in the target voxel as a function of the coil position is tent-shaped (blue line in Fig. 7a). The variance of 4.2% corresponds to a maximal distance of 8 mm of the two areas.

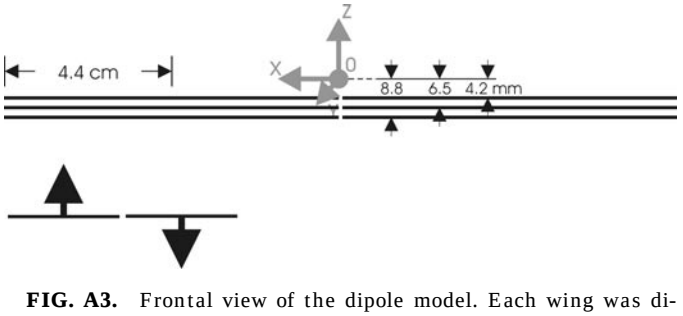


**FIG. A3.** Frontal view of the dipole model. Each wing was divided into three circular disks (top). The direction of the dipoles depends on the wing (bottom).

In the other case, the cortical areas were modeled to have linear input–output functions, followed by subcortical summation. This corresponds to sigmoidal functions at minimal steepness, resulting in an inverted U-shaped dependency of target voxel field strength on coil position (purple line in Fig. 7a). The maximal distance of the two areas resulting in a variance of 4.2% is 22 mm.

### Effects of a Distributed Area

A distributed area can be assumed to consist of several small dot-shaped areas. Consequently, the dependency of field strength in the target voxel on the coil position will also follow an inverted U-shaped function. More exact model calculations are not feasible, as no rational assumptions can be made about relative contribution of each of the dot-shaped areas to the muscle response. In order to estimate the maximal possible size of a distributed area, we can think of it as reduced to two isolated areas at its borders. Consequently, the maximal distance between the two areas given above also represents as well the maximal extension of a distributed area.

### Comparison with the Measured Variance

In Fig. 7b, the relative distribution of the field strength measured in the voxel of minimal variance is shown for the four subjects. No systematic correlation of stimulation site and field strength as predicted from the model calculations in Fig. 7a can be observed. Quadratic functions were fitted to the data in order to test for putative systematic trends. None of the fits yielded significant results (AT, $F(2,8) = 0.059$; $P = 0.94$; MV, $F(2,10) = 0.076$; $P = 0.93$; SaBe, $F(2,6) = 0.031$; $P = 0.97$; TK, $F(2,9) = 0.140$; $P = 0.87$).

### Electric Field Strength vs Spatial Derivative of the Induced Field

In cortical applications of magnetic stimuli it is commonly assumed that the electric field strength itself is the relevant feature determining the stimulation of the cortical tissue (assumption (i) Amassian *et al.*, 1992;

Ilmoniemi *et al.*, 1999). Consequently, we used the experimental strategy to search for the cortical point at which the variance of the field strengths over all coil positions is minimal. In contrast, when straight peripheral nerves are stimulated magnetically, nerve excitation is assumed to be caused by the spatial derivative of the electric field (Maccabee *et al.*, 1993). Whereas this view has been directly tested for straight peripheral nerves in physiological experiments (Maccabee *et al.*, 1993), with respect to cortical stimulation no direct evidence that field strength is the relevant parameter has yet been recorded. In order to rule out the possibility that the cortical stimulation site is determined by the spatial derivative of the electric field, the following model simulations were conducted.

In initial simulations, Gaussian noise was added to the stimulator output intensities of an idealized U-shaped function for half-maximal CMAP responses until the minimal variance of field strength on the cortex reached 4.2% (systematic deviations were excluded as discussed above). Then the induced field strength was calculated on a line beneath the line of coil positions and lying on the cortical surface (approximated by a hemisphere with a radius of 8 cm). For all stimulation sites, the field strengths on the line on the cortex are shown in Fig. 8a. As expected, they form shifted and scaled bell-shaped curves which intersect roughly at the point of minimal variance, here seen at 100 mm on the chosen cortex line (compare Fig. 3).

The calculation was repeated, but the derivative of the electric field was calculated along the structure of interest, i.e., along the chosen line. For all stimulation sites, the curves generated by the derivative are depicted in Fig. 8b. As can be seen, there is no central intersection point. Applying the minimal variance method results in a minimal variance value of 68%. The points of minimal variance are shifted from 100 mm (Fig. 8a) to 48 and 152 mm (Fig. 8b).

Taken together, the simulations clearly demonstrate that the use of the derivative does not allow one to identify a cortical stimulation point. Consequently, the U-shaped functions for half-maximal CMAP responses as measured in the experiment cannot result from cortical tissue sensitive to the derivative of the induced field, but rather stem from tissue sensitive to the electric field strength itself.

## ACKNOWLEDGMENTS

We thank Hans-Günther Nusseck for technical support, as well as Kuno Kirschfeld, Georg Grön, and Manfred Spitzer for fruitful discussions. Michael Erb and Wolfgang Grodd provided us with the anatomical MR pictures.

## REFERENCES

Amassian, V. E., Eberle, L., Maccabee, P. J., and Cracco, R. Q. 1992. Modelling magnetic coil excitation of human cerebral cortex with a peripheral nerve immersed in a brain-shaped volume conductor: the significance of fiber bending in excitation. *Electroenceph. Clin. Neurophysiol.* **85:** 291–301.

Bastings, E. P., Gage, H. D., Greenberg, J. P., Hammond, G., Hernandez, L., Santago, P., Hamilton, C. A., Moody, D. M., Singh, K. D., and Ricci, P. E. 1998. Co-registration of cortical magnetic stimulation and functional magnetic-resonance-imaging. *NeuroReport* **9:** 1941–1946.

Beisteiner, R., Windischberger, C., Lanzenberger, R., Edward, V., Cunnington, R., Erdler, M., Gartus, A., Streibl, B., Moser, E., and Deecke, L. 2001. Finger somatotopy in human motor cortex. *Neuroimage* **13:** 1016–1026.

Bohning, D. E., He, L., George, M. S., and Epstein, C. M. 2001. Deconvolution of transcranial magnetic stimulation (TMS) maps. *J. Neural Transm.* **108:** 35–52.

Branston, N. M., and Tofts, P. S. 1990. Transcranial magnetic stimulation. *Neurology* **40:** 1909.

Brasil-Neto, J. P., Cohen, L. G., Panizza, M., Nilsson, J., Roth, B. J., and Hallett, M. 1992. Optimal focal transcranial magnetic activation of the human motor cortex: Effects of coil orientation, shape of induced current pulse, and stimulus intensity. *J. Clin. Neurophysiol.* **9:** 132–136.

Brasil-Neto, J. P., McShane, L. M., Fuhr, P., Hallett, M., and Cohen, L. G. 1992. Topographic mapping of the human motor cortex with magnetic stimulation: Factors affecting accuracy and reproducibility. *Electroenceph. Clin. Neurophysiol.* **85:** 9–16.

Classen, J., Knorr, U., Werhahn, K. J., Schlaug, G., Kunesch, E., Cohen, L. G., Seitz, R. J., and Benecke, R. 1998. Multimodal output mapping of human central motor representation on different spatial scales. *J. Physiol.* **512:** 163–179.

Devanne, H., Lavoie, B. A., and Capaday, C. 1997. Input-output properties and gain changes in the human corticospinal pathway. *Exp. Brain. Res.* **114:** 329–338.

Eaton, H. 1992. Electric field induced in a spherical volume conductor from arbitrary coils. Application to magnetic stimulation and MEG. *Med. Biol. Eng. Comput.* **30:** 433–440.

Epstein, C. M., Schwartzberg, D. G., Davey, K. R., and Sudderth, D. B. 1990. Localizing the site of magnetic brain stimulation in humans [see comments]. *Neurology* **40:** 666–670.

Hallett, M. 2000. Transcranial magnetic stimulation and the human brain. *Nature* **406:** 147–150.

Hämäläinen, M. S., and Sarvas, J. 1989. Realistic conductivity geometry model of the human head for interpretation of neuromagnetic data. *IEEE Trans. Biomed. Eng.* **36:** 165–171.

Herwig, U., Padberg, F., Unger, J., Spitzer, M., and Schönfeldt-Lecuona, C. 2001. Transcranial magnetic stimulation in therapy studies: Examination of the reliability of "standard" coil positioning by neuronavigation. *Biol. Psychiatry* **50:** 58–61.

Hess, C. W., Mills, K. R., Murray, N. M., and Schriefer, T. N. 1987. Excitability of the human motor cortex is enhanced during REM sleep. *Neurosci. Let.* **82:** 47–52.

Ilmoniemi, R. J., Ruohonen, J., and Karhu, J. 1999. Transcranial magnetic stimulation—A new tool for functional imaging of the brain. *Crit. Rev. Biomed. Eng.* **27:** 241–284.

Kammer, T., Beck, S., Thielscher, A., Laubis-Herrmann, U., and Topka, H. 2001. Motor thresholds in humans. A transcranial magnetic stimulation study comparing different pulseforms, current directions and stimulator types. *Clin. Neurophysiol.* **112:** 250–258.

Kozel, F. A., Nahas, Z., deBrux, C., Molloy, M., Lorberbaum, J. P., Bohning, D., Risch, S. C., and George, M. S. 2000. How coil-cortex distance relates to age, motor threshold, and antidepressant response to repetitive transcranial magnetic stimulation. *J. Neuropsychiatry Clin. Neurosci.* **12:** 376–384.

Krings, T., Buchbinder, B. R., Butler, W. E., Chiappa, K. H., Jiang, H. J., Cosgrove, G. R., and Rosen, B. R. 1997. Functional magnetic-

resonance-imaging and transcranial magnetic stimulation—Complementary approaches in the evaluation of cortical motor function. *Neurology* **48:** 1406–1416.

Levy, W. J., Amassian, V. E., Schmid, U. D., and Jungreis, C. 1991. Mapping of motor cortex gyral sites non-invasively by transcranial magnetic stimulation in normal subjects and patients. *Electroenceph. Clin. Neurophysiol. Suppl.* **43:** 51–75.

Liu, R., and Ueno, S. 2000. Calculating the activating function of nerve excitation in inhomogeneous volume conductor during magnetic stimulation using the finite element method. *IEEE Trans. Magn.* **36:** 1796–1799.

Maccabee, P. J., Amassian, V. E., Eberle, L. P., and Cracco, R. Q. 1993. Magnetic coil stimulation of straight and bent amphibian and mammalian peripheral nerve in vitro: Locus of excitation. *J. Physiol.* **460:** 201–219.

McConnell, K. A., Nahas, Z., Shastri, A., Lorberbaum, J. P., Kozel, F. A., Bohning, D. E., and George, M. S. 2001. The transcranial magnetic stimulation motor threshold depends on the distance from coil to underlying cortex: A replication in healthy adults comparing two methods of assessing the distance to cortex. *Biol. Psychiatry* **49:** 454–459.

Mills, K. R., Boniface, S. J., and Schubert, M. 1992. Magnetic brain stimulation with a double coil: The importance of coil orientation. *Electroenceph. Clin. Neurophysiol.* **85:** 17–21.

Mills, K. R., and Nithi, K. A. 1997. Corticomotor threshold to magnetic stimulation—Normal values and repeatability. *Muscle Nerve* **20:** 570–576.

Oldfield, R. C. 1971. The assessment and analysis of handedness: The Edinburgh inventory. *Neuropsychologia* **9:** 97–113.

Pascual-Leone, A., Cohen, L. G., Brasil-Neto, J. P., and Hallett, M. 1994. Non-invasive differentiation of motor cortical representation of hand muscles by mapping of optimal current directions. *Electroenceph. Clin. Neurophysiol.* **93:** 42–48.

Penfield, W., and Rasmussen, T. 1950. *The Cerebral Cortex of Man: A Clinical Study of Localization and Function.* Macmillan, New York.

Ravazzani, P., Ruohonen, J., Grandori, F., and Tognola, G. 1996. Magnetic stimulation of the nervous-system—Induced electric-field in unbounded, semiinfinite, spherical, and cylindrical media. *Ann. Biomed. Engineer.* **24:** 606–616.

Rossini, P. M., Caltagirone, C., Castriotascanderberg, A., Cicinelli, P., Delgratta, C., Demartin, M., Pizzella, V., Traversa, R., and Romani, G. L. 1998. Hand motor cortical area reorganization in stroke—A study with fMRI, MEG and TCS maps. *NeuroReport* **9:** 2141–2146.

Roth, B. J., Saypol, J. M., Hallett, M., and Cohen, L. G. 1991. A theoretical calculation of the electric field induced in the cortex during magnetic stimulation. *Electroenceph. Clin. Neurophysiol.* **81:** 47–56.

Sarvas, J. 1987. Basic mathematical and electromagnetic concepts of the biomagnetic inverse problem. *Phys. Med. Biol.* **32:** 11–22.

Schieber, M. H. 2001. Constraints on somatotopic organization in the primary motor cortex. *J. Neurophysiol.* **86:** 2125–2143.

Stewart, L. M., Walsh, V., and Rothwell, J. C. 2001. Motor and phosphene thresholds: A transcranial magnetic stimulation correlation study. *Neuropsychologia* **39:** 415–419.

Terao, Y., Ugawa, Y., Sakai, K., Miyauchi, S., Fukuda, H., Sasaki, Y., Takino, T., Hanajima, R., Furubayashi, T., Pütz, B., and Kanazawa, I. 1998. Localizing the site of magnetic brain-stimulation by functional MRI. *Exp. Brain. Res.* **121:** 145–152.

Thickbroom, G. W., Sammut, R., and Mastaglia, F. L. 1998. Magnetic stimulation mapping of motor cortex-factors contributing to map area. *Electroenceph. Clin. Neurophysiol.* **109:** 79–84.

Walsh, V., and Cowey, A. 2000. Transcranial magnetic stimulation and cognitive neuroscience. *Nat. Rev. Neurosci.* **1:** 73–79.

Wassermann, E. M., McShane, L. M., Hallett, M., and Cohen, L. G. 1992. Noninvasive mapping of muscle representations in human motor cortex. *Electroenceph. Clin. Neurophysiol.* **85:** 1–8.

Wassermann, E. M., Wang, B. S., Zeffiro, T. A., Sadato, N., Pascual-leone, A., Toro, C., and Hallett, M. 1996. Locating the motor cortex on the MRI with transcranial magnetic stimulation and PET. *NeuroImage* **3:** 1–9.

Wilson, S. A., Thickbroom, G. W., and Mastaglia, F. L. 1993. Transcranial magnetic stimulation mapping of the motor cortex in normal subjects. The representation of two intrinsic hand muscles. *J. Neurol. Sci.* **118:** 134–144.

Yousry, T. A., Schmid, U. D., Alkadhi, H., Schmidt, D., Peraud, A., Buettner, A., and Winkler, P. 1997. Localization of the motor hand area to a knob on the precentral gyrus—A new landmark. *Brain* **120:** 141–157.